Inorganic Chemistry

Article

pubs.acs.org/IC

A Collection of Topological Types of Nanoclusters and Its Application to Icosahedron-Based Intermetallics

Arina A. Pankova,[†] Tatiana G. Akhmetshina,[†] Vladislav A. Blatov,*[,†] and Davide M. Proserpio[†,‡]

[†]Samara Center for Theoretical Materials Science (SCTMS), Samara State University, Ac. Pavlov St. 1, Samara 443011, Russia

[‡]Dipartimento di Chimica, Università degli Studi di Milano, Via Golgi 19, 20133 Milano, Italy

Supporting Information

ABSTRACT: In this study, we carried out a topological and geometrical analysis of more than 27 000 intermetallics. More than 2000 topologically different nanoclusters were determined and stored in an electronic database as the Topological Types of Nanoclusters (TTN) collection. Besides the topology of the nanoclusters, the TTN collection contains the information on their occurrence as well as on motifs of their assembly in intermetallics; it is included to the set of the ToposPro topological collections. With the TTN collection we analyzed the topology of local binding and overall topological motifs in the 1528 intermetallics assembled with icosahedron-based building units. Taking the TTN collection as a starting point, we present the concept of a knowledge database and an expert system that can be used to process a huge set of data to find general regularities in the crystal structures of intermetallics and to predict some of their features.

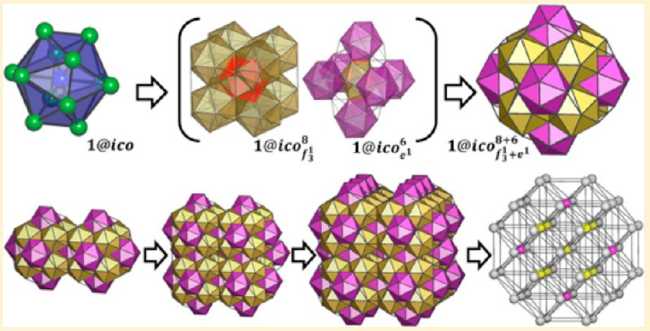

INTRODUCTION

Many crystal structures of intermetallics are rather simple and can be easily described as close-packed layers[1] or cluster ensembles[2−6] or in terms of atomic coordination polyhedra.[7,8] However, there are quite complicated structures with hundreds or even thousands of atoms in the unit cell; it has always been a challenge for inorganic crystal chemistry to rationalize them. Because of the lack of universal criteria for identification of building units in such intermetallics, their structure description can be quite arbitrary. As a result, the same structure can be described in several different ways[9−17] that are not commonly accepted; altogether, this has hindered the process of establishing structural relations between intermetallics.

While the models of close-packed layers or coordination polyhedra were known in crystal chemistry of intermetallics long ago, the cluster models have gained particular importance in the last decades thanks to a growing interest in nanoclusters and quasicrystals.[18−20] Up to now, quantum-mechanical methods have been successfully used to model isolated clusters using various optimization algorithms,[21−25] providing the global minimum potential energy conformations of the clusters. Many of the results obtained have been gathered in the Cambridge Cluster Database,[26] which lists the lowest values of energies and appropriate conformations for a wide range of clusters obtained at different interaction potentials. At the same time, this database does not provide any information on the cluster connectivity (i.e., all topological properties of the clusters remain unknown) or the occurrence of the clusters in nature.

Another way to describe crystal structures is based on modeling methods that rest upon comprehensive geometrical and topological analysis by application of the concept of infinite graphs.[27] Topological approaches consider the connectivity of building units to characterize the topology of underlying nets that provide a deeper understanding of the crystal structure assembly. That is why the topological methods have gained an important role in exploring intermetallic crystal structures. We recently proposed the nanocluster method to describe any intermetallic compound following a strict algorithm of searching for the structural units (*nanoclusters*) that assemble the entire crystal structure.[28,29] This method is based on the idea that the crystal structure is formed by means of self-assembly of the nanoclusters corresponding to optimal (*fundamental*) configurations of atoms.

In this paper, we apply the nanocluster method to analyze all known intermetallic compounds and to build a database of the nanoclusters that compose their crystal structures. We show how this database can be used to explore a particular class of intermetallics, namely, the structures assembled with icosahedron-based building units. We also outline the possibility of developing an expert system for predicting intermetallic structures by introducing a number of descriptors that characterize the chemical composition and geometrical and topological properties of the nanoclusters as well as motifs of their assembly in the intermetallic architectures.

EXPERIMENTAL SECTION

Objects and Principles of the Nanocluster Analysis. The objects of our investigation are intermetallics composed by the metal

Received: April 29, 2015
Published: June 11, 2015

DOI: 10.1021/acs.inorgchem.5b00960
Inorg. Chem. 2015, 54, 6616−6630

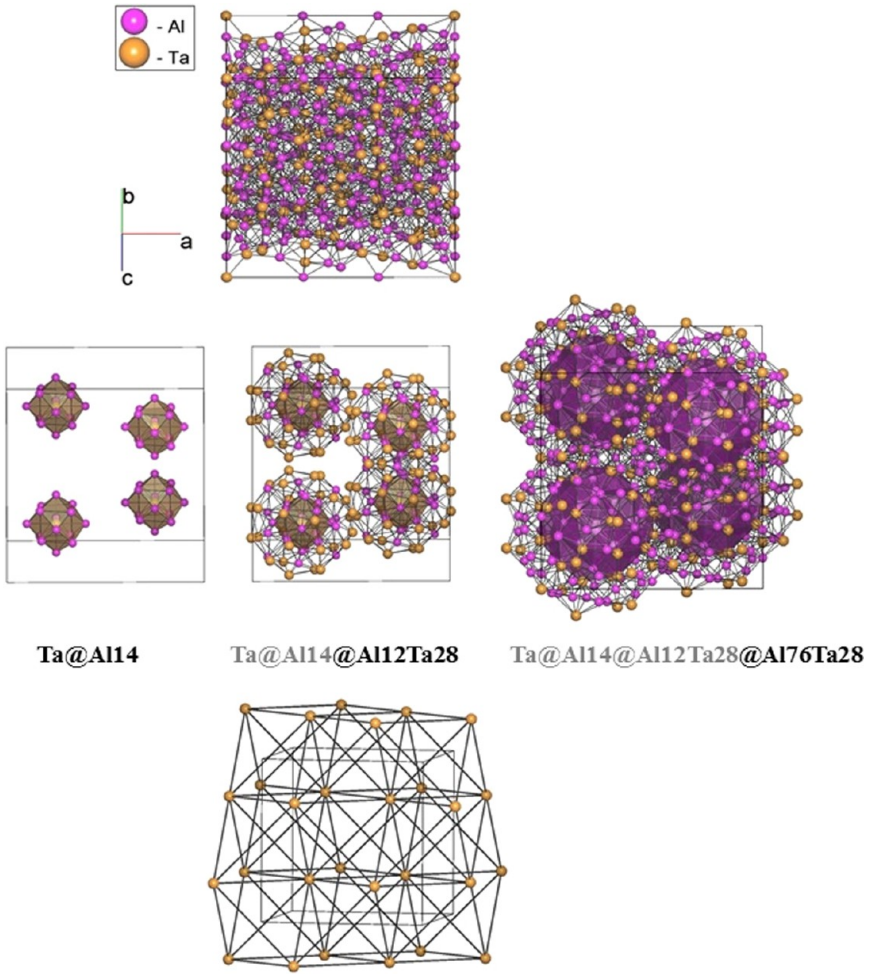

Figure 1. (top) Atomic net in the $Al_{69}Ta_{39}$ structure.[34] (middle) Shells of the Ta@Al14@Al12Ta28@Al76Ta28 primary nanocluster: (left) first shell; (center) second shell; (right) third shell. (bottom) Face-centered cubic underlying net (**fcu**) of the three-shell primary nanoclusters.

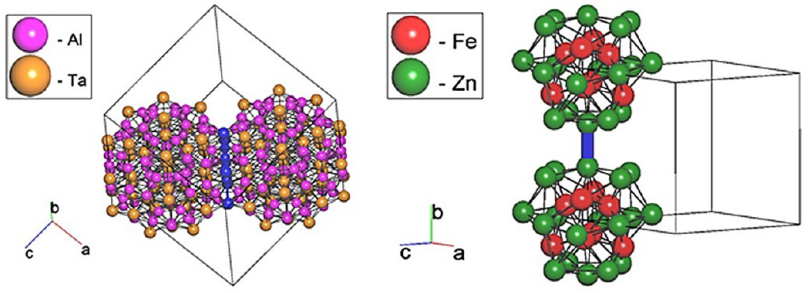

Figure 2. Two noninterpenetrating nanoclusters: (a) Ta@Al14@Al12Ta28@Al76Ta28 nanoclusters in the $Al_{69}Ta_{39}$ crystal structure interconnected by common atoms (in blue); (b) 0@Fe4@Fe4Zn18 nanoclusters in the $Fe_{13}Zn_{39}$ crystal structure connected by an intercluster bond (in blue).

atoms placed below the Zintl line in the periodic table. The crystallographic data were taken from the Inorganic Crystal Structure Database (ICSD, release 2014/2) and Pearson's Crystal Data (version 2010/2011). A total of more than 27 000 crystal structures were considered, and the nanocluster method was applied to all of them to find the structural units from which they are assembled.

The nanocluster method is based on the following principles:

(i) Crystal structures of intermetallics are formed as an assembly of matryoshka-like (onion) polyshell *primary* nanoclusters (Figure 1). We emphasize that the nanoclusters are represented as their graphs, i.e., the connectivity of the atoms is considered along with their geometrical configuration. The interconnected centers of the primary nanoclusters form an *underlying net* that describes the topology of the nanocluster assembly (Figure 1 bottom). In this paper, we denote the underlying nets with bold three-letter symbols of the Reticular Chemistry Structure Resource (RCSR) nomenclature.[30]

(ii) The centers of primary nanoclusters occupy the highest-symmetry positions of the structure.

(iii) The primary nanoclusters are usually centered with highly coordinated atoms. However, the nanocluster can also be "empty" (noncentered) if it obeys the previous principles.

(iv) The primary nanoclusters do not interpenetrate (Figure 2), i.e., they have no common internal atoms. The connectivity of the nanoclusters can be realized through intercluster bonds (b) or through common vertices (v), edges (e), or faces (f) by sharing of surface atoms.

DOI: 10.1021/acs.inorgchem.5b00960
Inorg. Chem. 2015, 54, 6616−6630

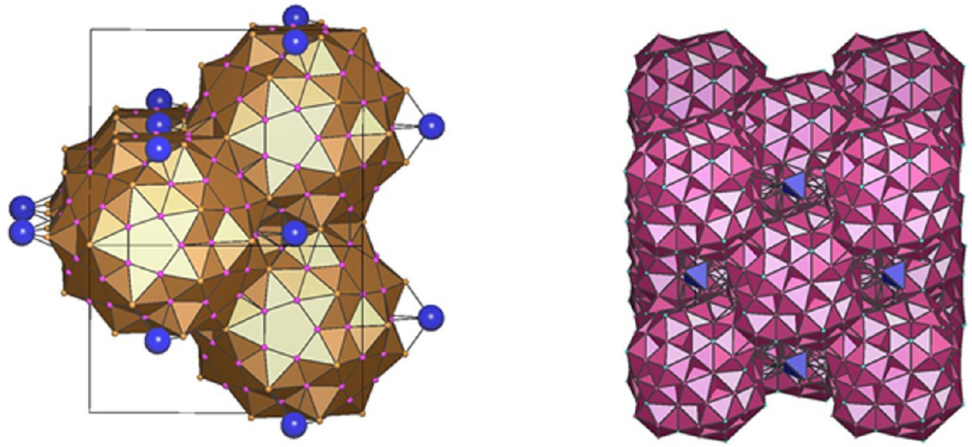

Figure 3. (left) Ta(2) atoms (in blue) filling the space between the Ta@Al14@Al12Ta28@Al76Ta28 nanoclusters in the $Al_{69}Ta_{39}$ crystal structure. (right) Tetrahedral Sc_4 spacers (in blue) in the $Sc_{44}Os_7$ crystal structure formed by the 0@Os4Sc4@Sc34@Os24Sc72 nanoclusters.

(v) The primary nanoclusters should include all of the atoms in the structure. Along with the primary nanoclusters, the structure may contain single atoms or small groups of atoms that fill voids between the primary nanoclusters (Figure 3). We call such interstitial species *spacers*.

(vi) The *parsimony* condition implies that the size and number of the primary nanoclusters should be minimal.

These rules have been implemented in the ToposPro program package[29] as the "Nanoclustering" procedure;[28] a number of applications of the approach have been discussed elsewhere.[31−33]

Analysis Algorithm. The algorithm for geometric and topological analysis of intermetallics with the ToposPro program package includes the following steps:

(a) Calculation of the adjacency matrix of the crystal structure using the AutoCN program. We take into account the interatomic interactions corresponding to the faces of atomic Voronoi polyhedra with solid angles (Ω) no less than 1.5% of 4π steradians. This geometrical approach allows us to avoid ambiguity when determining interatomic contacts; it showed its effectiveness for the analysis of connectivity in intermetallics.[31−33] As a result, we obtain a net of the whole structure, where the nodes and edges correspond to the atoms and contacts between them. We emphasize that this net model does not imply that the contacts between the atoms are directed or pairwise; the nature of the bonding is not of concern here. The net just approximates the structure connectivity and allows us to analyze many topological properties of both the whole structure and separate structural units. In particular, the topologies of all of the polyhedra and nanoclusters discussed below are unambiguously determined as the corresponding graphs once the structure net is built; the same concerns all operations on the next steps.

(b) Decomposition of the entire structure to nanoclusters with the "Nanoclustering" procedure.

(c) Construction of the underlying net of the nanoclusters and determination of the underlying net topology using the ADS program.

(d) Search for the nanocluster graph in the atomic nets of other intermetallics using the algorithm for selecting finite subgraphs in infinite periodic graphs.[28] If such a nanocluster fragment does not obey principles (i)−(vi) of the nanocluster approach, we call it a *local atomic configuration*. However, if the local atomic configuration is constructed according to principle (i) but may fit other principles, we call it a *nanocluster configuration*. In both cases, the word "configuration" stresses that this is not a building unit of the crystal but just a special group of atoms that is stable for some reason. A simple example of a nanocluster configuration is an atom together with its first coordination shell (a coordination polyhedron).

RESULTS AND DISCUSSION

Collection of Topological Types of Nanoclusters. To provide a systematic structural description of intermetallics with the nanocluster approach, we have created the Topological Types of Nanoclusters (TTN) collection, which contains information about all possible topological types of nanoclusters and their occurrence in more than 27 000 intermetallics under consideration. The TTN collection is included in the set of the ToposPro topological collections[29] and comprises the data on 1006 polyhedral (single-shell) and 1011 multishell nanoclusters that occur as local atomic configurations and/or primary nanoclusters in the intermetallic structures. This database provides information on the topology of the nanoclusters and their chemical composition and occurrence (Scheme 1). In

Scheme 1. Content of the Topological Types of Nanoclusters (TTN) Collection

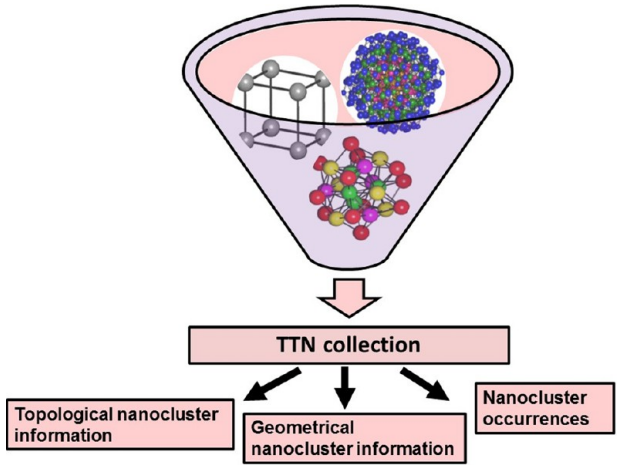

turn, the topological data include the nanocluster graph as well as the number and compositions of its shells. The nanocluster symbol is written in the form $N_0@N_1@N_2\cdots$, where N_0, N_1, N_2, ... are the numbers of atoms in the subsequent shells; the origin atom forms the zeroth shell. Topologically different nanoclusters with the same $N_0@N_1@N_2\cdots$ symbol are distinguished

DOI: 10.1021/acs.inorgchem.5b00960
Inorg. Chem. 2015, 54, 6616−6630

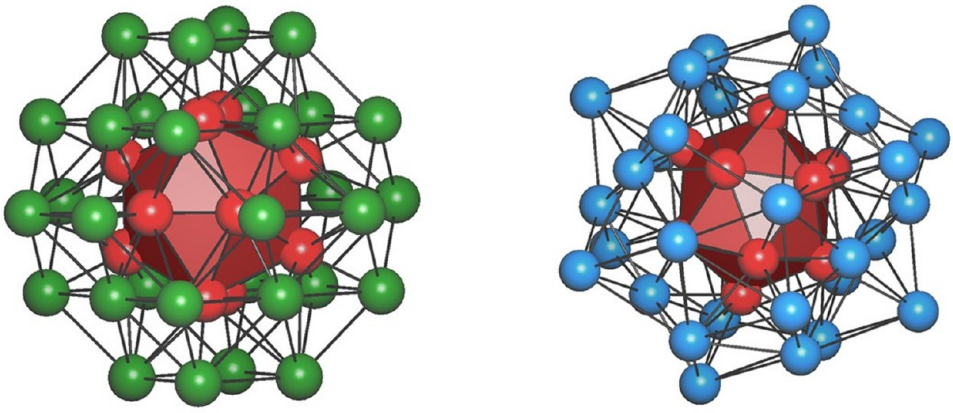

Figure 4. Two 1@12@32-type nanoclusters: (left) 1@12@32_model1 of the Hg@Hg12@Hg20Rb12 composition in the Rb_3Hg_{20} crystal structure; (right) 1@12@32_model3 of the Tl@Tl12@K26Na6 composition in the $Na_3K_8Tl_{13}$ crystal structure.

as model1, model2, etc. For example, the 1@12@32-type nanoclusters occur in four different topologies, two of which, 1@12@32_model1 and 1@12@32_model3, are shown in Figure 4. Both nanoclusters are centered and have two shells consisting of 12 and 32 atoms, but their graphs are different. In particular, the 1@12@32_model1 nanocluster occurs as a local atomic configuration and as a primary nanocluster in 25 and two intermetallics, respectively.

The TTN collection is an example of a second-level database,[35] which contains knowledge (structure parameters) extracted from information in crystallographic (first-level) databases such as the ICSD and Pearson's Crystal Data. To create a full-fledged knowledge database that can be used in structure prediction, we need additional data, namely, the database of relations between the parameters stored in the TTN collection. Below we consider how such relations can be found, using the example of intermetallic structures built with a well-known structural unit: the icosahedron.

Icosahedra as Building Units in Intermetallics. The icosahedron as a primary nanocluster can be of two types: empty (0@12) or centered (1@12). In both cases, the icosahedron (*ico*; all symbols for polyhedra are taken from the RCSR[27]) is a 12-vertex convex polyhedron with 30 edges (which correspond to interatomic contacts) and 20 triangular faces. In total, the TTN collection contains 72 and 14 topologically different centered and empty 12-vertex clusters, respectively, among which the centered icosahedron 1@12_model1 and the empty icosahedron 0@12_model12 occupy the sixth and seventh places by occurrence, respectively (highlighted in yellow in Table S1 in the Supporting Information).

Nanocluster analysis of the 3600 intermetallics containing empty or centered icosahedra as nanocluster configurations revealed 1528 crystal structures completely assembled from icosahedra as the primary nanocluster; an overwhelming majority of them (1506) are built of just one kind of icosahedron. With the ToposPro classification procedure, we have arranged these 1528 intermetallics into 43 topological types; all of the structures within the same topological type have isomorphic atomic nets. This means that the topological properties of the structures belonging to the same topological type are equivalent and only one representative from the type can be used in the subsequent topological analysis.

Local and Overall Topologies of Icosahedron-Based Motifs. To find more correlations between the 1528 intermetallics, we have considered the topologies of the underlying nets, where the net nodes coincide with the centers of mass of the icosahedra, while the net edges correspond to links between the icosahedra. The group of condensed icosahedra can be considered as the next level of the structure local organization, a *supracluster*. To describe the method of local binding (LB) of nanoclusters, not only icosahedra, we have introduced the supracluster descriptor $\text{Center@shell}^{\text{CN}}_{v,e,f,b}$, where Center = 0 or 1 for an empty or centered icosahedron, respectively; shell is a symbol for the shell type; and CN is the coordination number of the central nanocluster, represented as a sum $a_1 + a_2 + a_3 + \ldots$, where a_1, a_2, a_3, ... are numbers of nanoclusters connected to the central one in the same manner. The modes of linking of adjacent icosahedra by common vertices, edges, faces, and intercluster bonds were described by Shoemaker and Shoemaker;[36] we designate these types of connection by the *v*, *e*, *f*, and *b* symbols, respectively. The number of contacts of a given connection type is specified by a superscript after the letter *v*, *e*, *f*, or *b*; in addition, *f* has a subscript that is equal the number of face vertices. Intercluster bonds (type *b*) are specified only if the nanoclusters have no common atoms. For example, the $TaCo_2$ crystal structure[37] can be presented as an assembly of atom-centered icosahedra (1@*ico*). The local icosahedra binding for this structure has the topology $1@ico^{1+3+6}_{f_3^1+v^1+e^1}$, where the central atom-centered icosahedron is connected to one icosahedron through one triangular face ($1@ico^1_{f_3^1}$), to three icosahedra through one common vertex ($1@ico^3_{v^1}$), and to the remaining six icosahedra through one edge ($1@ico^6_{e^1}$) (Figure 5), resulting in the 10-coordinated (10-c) **tca** net. Tables S2 and S3 in the Supporting Information show that the 1528 intermetallics can differ with respect to underlying nets and/or local binding of icosahedra (LB*ico*).

Intermetallics Assembled from One Kind of Icosahedron. General distributions of the 1506 icosahedron-based intermetallics (32 topological types) based on the types of local binding of the icosahedra and their overall binding motifs (underlying nets) are given in Tables 1 and 2, respectively. The distributions show that the LB*ico* $1@ico^{2+6}_{f_3^1+e^1}$ and $1@ico^{8+6}_{f_3^1+e^1}$ with the 8-coordinated **hex** and 14-coordinated **bcu-x** underlying nets, respectively, are the most common in the icosahedron-based intermetallic compounds, although some other types of connection are also rather abundant. Below we discuss in detail the most important topological types of icosahedron-based architectures, drawing special attention to correlations between the local and overall architectures.

DOI: 10.1021/acs.inorgchem.5b00960
Inorg. Chem. 2015, 54, 6616−6630

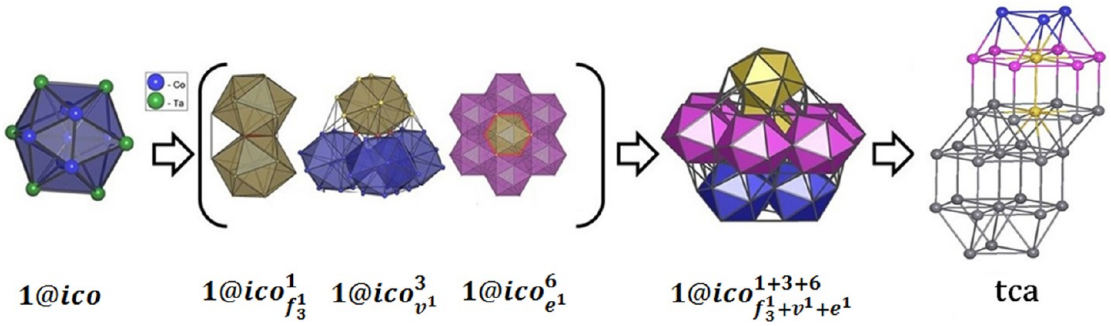

Figure 5. Crystal structure of $TaCo_2$: (left) an atom-centered 1@12 icosahedron; (middle) the constituents of the 1@ico$^{1+3+6}_{f_3^1+v^1+e^1}$ supracluster, where the central icosahedron is connected to the surrounding ones through faces, vertices, and edges; (right) the resulting **tca** underlying topology. Hereinafter, the centers of the supracluster constituents are highlighted in the underlying net with the corresponding colors.

Table 1. Distribution of the Local Nanocluster Binding in Intermetallics

LB*ico*	underlying net	no. of structures	percentage (%)
1@ico$^{2+6}_{f_3^1+e^1}$	8-c **hex**	766	50.9
1@ico$^{8+6}_{f_3^1+e^1}$	14-c **bcu-x**	427	28.4
1@ico$^{6}_{f_3^1}$	6-c **crs**	100	6.6
1@ico$^{1+3+6}_{f_3^1+v^1+e^1}$	10-c **tca**	81	5.4
1@ico$^{2+2+4}_{f_3^1+e^1+v^1}$	8-c **hex**	39	2.6
1@ico$^{3+6}_{f_3^1+e^1}$	9-c **ncb**	22	1.5
others		71	4.6

Table 2. Distribution of the Topologies of the Underlying Nets

centered *ico*			empty *ico*		
overall topology	no. of structures	percentage (%)	overall topology	no. of structures	percentage (%)
hex	809	54.0	**hex**	7	77.8
bcu-x	437	29.2	**lcy**	1	11.1
crs	100	6.7	**bcu-x**	1	11.1
tca	81	5.4			
ncb	22	1.5			
pcu	19	1.3			
fcu	14	0.9			
hxl	7	0.5			
dia	5	0.3			
($3^6.4^{12}.5^3$)	2	0.1			
sql	1	0.1			

*14-Coordinated **bcu-x** Underlying Net (437 Entries).* As shown in Table S2 in the Supporting Information, the local nanocluster binding for the structures with the extended (8 → 14)[30] 14-coordinated **bcu-x** underlying net has the topology 1@ico$^{8+6}_{f_3^1+e^1}$, 1@ico$^{8+6}_{b^6+b^2}$, or 1@ico$^{2+8+4}_{e^1+b^4+b^1}$. The most frequent of these, 1@ico$^{8+6}_{f_3^1+e^1}$ coordination of icosahedra (it occurs in 427 crystal structures of the Mo_3Zr topological type[38]), and the subsequent assembly as a successive condensation of such superclusters into chains, layers, and finally a framework, which predetermine the underlying net of the whole structure, are shown in Figure 6. The icosahedra are packed into 1@ico$^{8+6}_{b^6+b^2}$ supraclusters in nine structures of the WAl_{12} topological type[39] (Figure 7 top) and in the only structure, $Nb(Cu_{0.5}Ga_{0.5})$,[40] where the 1@ico$^{2+8+4}_{e^1+b^4+b^1}$ is realized (Figure 7 bottom). The WAl_{12}-type structures are the only example of the so-called *nanocluster packings*,[28] where the nanoclusters have no common atoms and hence the chemical composition of the nanocluster and the whole structure coincide (W@Al12).

*12-Coordinated **fcu** Underlying Net (14 Entries).* Atom-centered icosahedra are rarely packed according to the face-centered cubic (**fcu**) motif. The topologies of the local binding of icosahedra with a 12-coordinated underlying net are 1@ico$^{12}_{v^1}$, 1@ico$^{6+6}_{f_3^2+e^1}$, and 1@ico$^{6+6}_{f_3^1+v^1}$, which occur in the ternary systems of the $CeRu_2Mg_5$[41] (one entry), Cu_2GaSr[42] (two entries), Ni_2SrGe[43] (one entry), and Ni_2BaGe[44] (one entry) topological types and in the binary systems of the $AlAu_4$ topological type[45] (nine entries) (Figure 8).

*10-Coordinated **tca** Underlying Net (81 Entries).* The arrangement of 10 icosahedra surrounding the central atom-centered icosahedron corresponds to the 10-coordinated **tca** underlying net in the 81 structures of the $TaCo_2$ topological type.[37] The local binding of icosahedra for these structures has the unique 1@ico$^{1+3+6}_{f_3^1+v^4+e^1}$ topology, as was described above (Figure 8).

*9-Coordinated **ncb** Underlying Net (22 Entries).* A 9-coordinated underlying net of atom-centered icosahedra corresponds to the **ncb** motif for eight structures of the Ni_4Zn_{22} topological type[46] and 14 structures for the Cu_5Zn_8[47] topological type with the 1@ico$^{3+6}_{f_3^1+v^1}$ topology of the local binding of icosahedra (Figure 9 top). It should be noted that the structures of the Ni_4Zn_{22} type can also be constructed as a condensation of the γ-brass 0@4@22 clusters, which were discovered by Brandon et al. in Cu_5Zn_8.[47] This alternative description exists thanks to interpenetration of four icosahedra, whose barycenters coincide with the vertices of the outer tetrahedron of the γ-brass structure.[48] The structures of the Ni_4Zn_{22} type are packed with the γ-brass clusters according to the **bcu-x** motif with the γ-brass$^{8+6}_{f_3+b^{13}}$ local topology (Figure 9 bottom). Here we see that the same structure can be represented with several nanocluster models. Which of them is the best one? The question is incorrect; all models can be used to search for correlations between different structures. We recently showed how different γ-brass-type intermetallics relate to each other;[31] now we see how some of them are involved in the icosahedron-based motifs.

*8-Coordinated **hex** Underlying Net (809 Entries).* Another method of connecting atom-centered 1@12 icosahedra was revealed in the 807 structures of the WBe_2[49] (758 entries), Fe_2Ta[37] (eight entries), $PuCu_6$[50] (39 entries), K_2Hg_7[51] (two entries), and Co_2Al_5[52] (two entries) topological types. In these structures, the 1@12 icosahedra are assembled according to a 8-coordinated hexagonal primitive lattice (**hex**) motif and have four possible LB*ico* topologies: 1@ico$^{2+6}_{f_3^1+e^1}$ (WBe_2 and Fe_2Ta), 1@ico$^{2+6}_{b^{12}+e^1}$ (K_2Hg_7), 1@ico$^{2+2+4}_{f_3^1+e^1+v^1}$ ($PuCu_6$), and 1@ico$^{2+6}_{f_3^1+b^4}$

DOI: 10.1021/acs.inorgchem.5b00960
Inorg. Chem. 2015, 54, 6616−6630

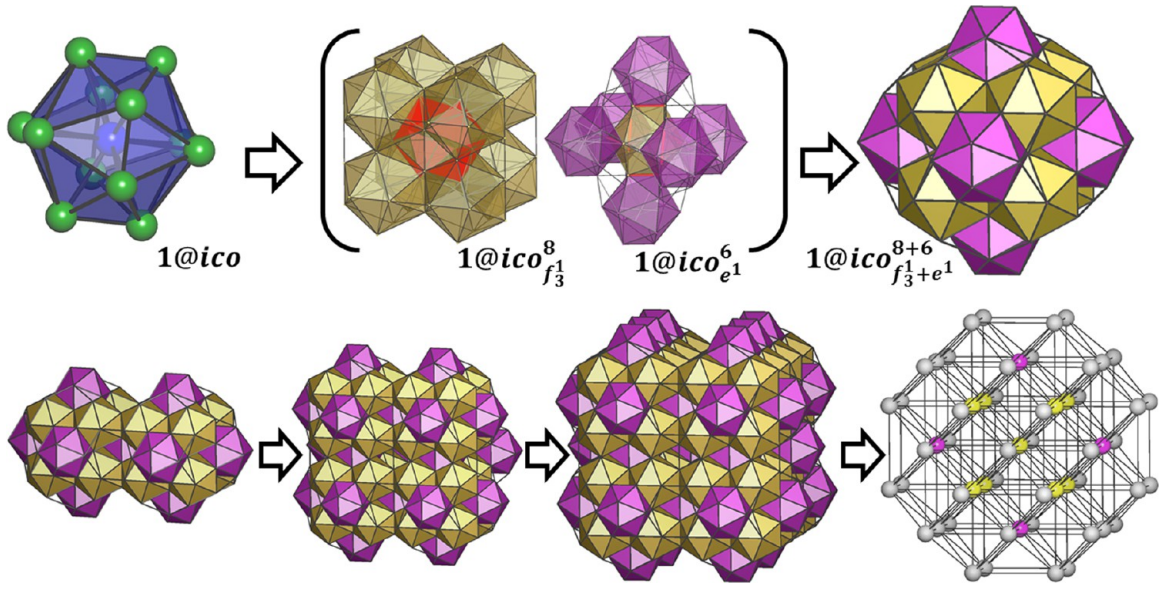

Figure 6. Mo_3Zr crystal structure: (top) an atom-centered 1@12 icosahedron (left) and the constituents (middle) of the $1@ico^{8+6}_{f_3^1+e^1}$ supracluster (right), where the central icosahedron (highlighted in red) is connected to the surrounding ones through faces and edges; (bottom) condensation of the $1@ico^{8+6}_{f_3^1+e^1}$ supraclusters into a chain, a layer, and a framework of a 14-c **bcu-x** underlying topology.

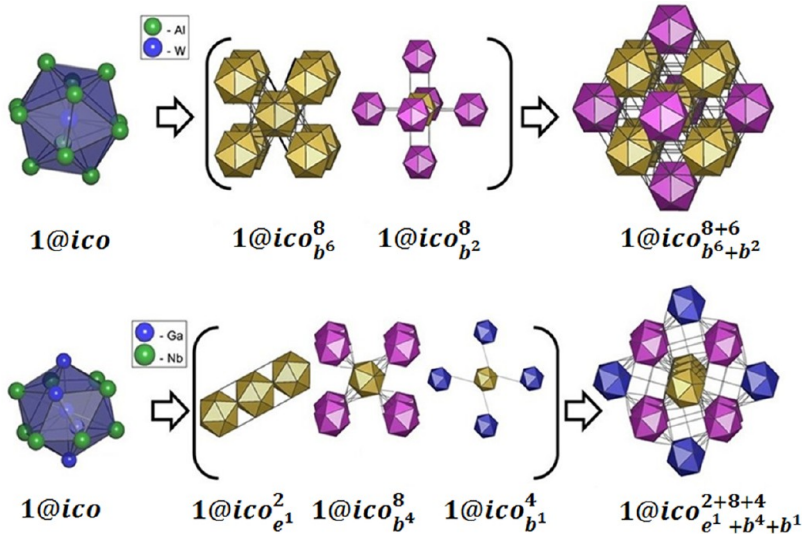

Figure 7. (top) The WAl_{12} crystal structure: an atom-centered 1@12 icosahedron (left) and the constituents (middle) of the $1@ico^{8+6}_{b^6+b^1}$ supracluster (right), where the central icosahedron is connected to the surrounding ones only by intercluster bonds. (bottom) The $Nb(Cu_{0.5}Ga_{0.5})$ crystal structure: an atom-centered 1@12 icosahedron (left) and the constituents (middle) of the $1@ico^{2+8+4}_{e^1+b^4+b^1}$ supracluster (right), where the central icosahedron is connected to the surrounding ones through edges and bonds.

(Co_2Al_5). In the WBe_2 and Fe_2Ta types, each atom-centered 1@12 icosahedron is surrounded by two icosahedra through a triangular face and by six icosahedra through an edge (Figure 10 top). The $1@ico^{2+6}_{b^{12}+e^1}$ supracluster in K_2Hg_7 is constructed as a condensation of two and six icosahedra connected to the central one by 12 bonds and one common edge, respectively (Figure 10 middle). In the $CeCu_6$ structure, the central icosahedron is condensed with two icosahedra through a triangular face, with two icosahedra through an edge, and with four icosahedra through a common vertex (Figure 10 bottom).

New 7-Coordinated Underlying Net (Two Entries). A new 7-coordinated uninodal net topology of distorted atom-centered icosahedra (point symbol $3^6.4^{12}.5^3$) was found in the $NdTi_3(Sn_{0.1}Sb_{0.9})_4$ and $SmTi_3(Sn_{0.1}Sb_{0.9})_4$ crystal structures;[53] the corresponding local coordination is described by the $1@ico^{3+4}_{e^1+v^1}$ symbol (Figure 11). The 7-coordinated $1@ico^{3+4}_{e^1+v^1}$ supraclusters are assembled in layers, and the systems of bonds between these layers lead to a three-dimensional framework.

6-Coordinated Underlying Nets (127 Entries). The 6-coordinated **crs**, **pcu**, **hxl**, and **lcy** underlying nets of icosahedra occur in 127 crystal structures. The **crs** underlying nets are composed of the $1@ico^{6}_{f_3^1}$ supraclusters in the Ti_2Ni[54] (68 entries) and Gd_4RhIn[55] (32 entries) topological types (Figure 12 left). Another example of the atom-centered icosahedra assembly with the $1@ico^{6}_{f_3^1}$ supracluster corresponds to the primitive cubic (**pcu**) motif that exists in the Ca_3Ag_8 topological type[56] (19 entries) (Figure 12 middle). As shown from Figure 12, the

DOI: 10.1021/acs.inorgchem.5b00960
Inorg. Chem. 2015, 54, 6616−6630

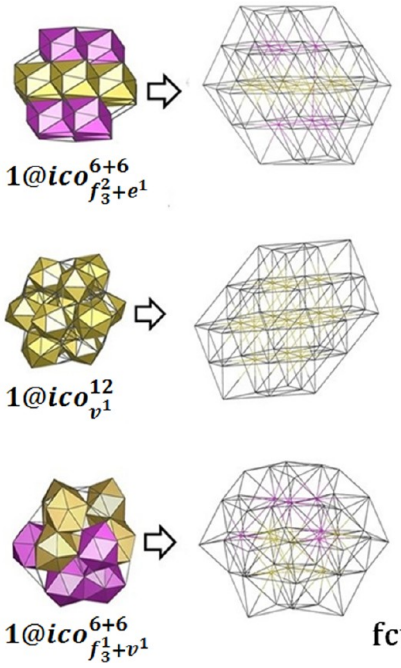

Figure 8. (left) Supraclusters of different types and (right) the corresponding face-centered (**fcu**) underlying nets: $1@ico^{12}_{v^1}$ in $CeRu_2Mg_5$ (top); $1@ico^{6+6}_{f_3^2+e^1}$ in Cu_2GaSr (middle); $1@ico^{6+6}_{f_3^1+v^1}$ in $AlAu_4$ (bottom).

topologies of the $1@ico^6_{f_3^1}$ supraclusters are different in the **crs**- and **pcu**-based architectures; we call such phenomenon *local topological isomerism*. The same LB*ico* type but for noncentered icosahedra ($0@ico^6_{f_3^1}$) results in the **lcy** underlying net in the $Y_5Ag_3Cu_{12}$ topological type[57] (Figure 12 right).

If we consider only connections with shared atoms of icosahedra, then different 6-coordinated supraclusters can be separated: $1@ico^6_{f_3^2}$ in Sr_2Ni_3;[58] $1@ico^{4+2}_{v^1+e^1}$ in Yb_2Ag_7,[59] Ca_2Ag_7,[60] Hf_2Co_7,[61] and Zr_2Ni_7;[62] $1@ico^{4+2}_{f_3^1+e^1}$ in $Al_{2.88}Ta_{2.66}V_{1.46}$,[63] and $1@ico^{2+4}_{f_3^2+e^1}$ in $Sr_2Rh_2In_3$.[64] In all cases, such supraclusters assemble **hxl** layers; however, there are additional bonds between the icosahedra that merge these layers into three-dimensional frameworks; full LB*ico* are shown in Figure 13.

In addition, the Ti_2Ni, Gd_4RhIn, and Ca_3Ag_8, structures have alternative models of their assembly with the Ti_2Ni-type[54] or γ-brass-type clusters,[47] but discussion of these models lies beyond the scope of this article.

Using the TTN collection and the "Nanoclustering" procedure, we have observed that icosahedron-based nanoclusters are frequently encountered in intermetallics. It was interesting to know how often such models were mentioned by the authors of the original structure investigations. A detailed analysis revealed the following four cases:

(i) The authors' and nanocluster models are identical only for the $ReAl_{12}$ structure type, where a body-centered-cubic packing of icosahedra was found.[65]

(ii) For five topological types, the authors mentioned icosahedra as structural units; however, in most cases the original description did not consider the local or overall topology of their bindings. The exception is Ca_3Ag_8, where a diagonal connection of icosahedra in the cubic lattice was discussed.[55]

(iii) For 10 topological types, the authors proposed quite different models that do not include icosahedra as structural units. For instance, the authors of ref 53 described the structure of $LnTi_3(Sn_xSb_{1-x})_4$ (Ln = Nd, Sm) as slabs of $TiSb_6$ octahedra stacked with nets of Nd atoms, while we have detected disordered Ti@Ti4Nd2Sb6 and Ti@Ti4Sm2Sb6 icosahedra (Figure 11) as the building units.

(iv) The authors of the original papers did not provide any cluster representation for 11 topological types.

In general, this comparison shows that topological models are still not popular in the crystal chemistry of intermetallics; in most cases, the authors do not go beyond the first coordination shell of atoms in the analysis of the compound architecture.

Intermetallics Assembled from Two or More Kinds of Icosahedra. We now briefly discuss the 22 intermetallics (eight topological types) that are constructed from several

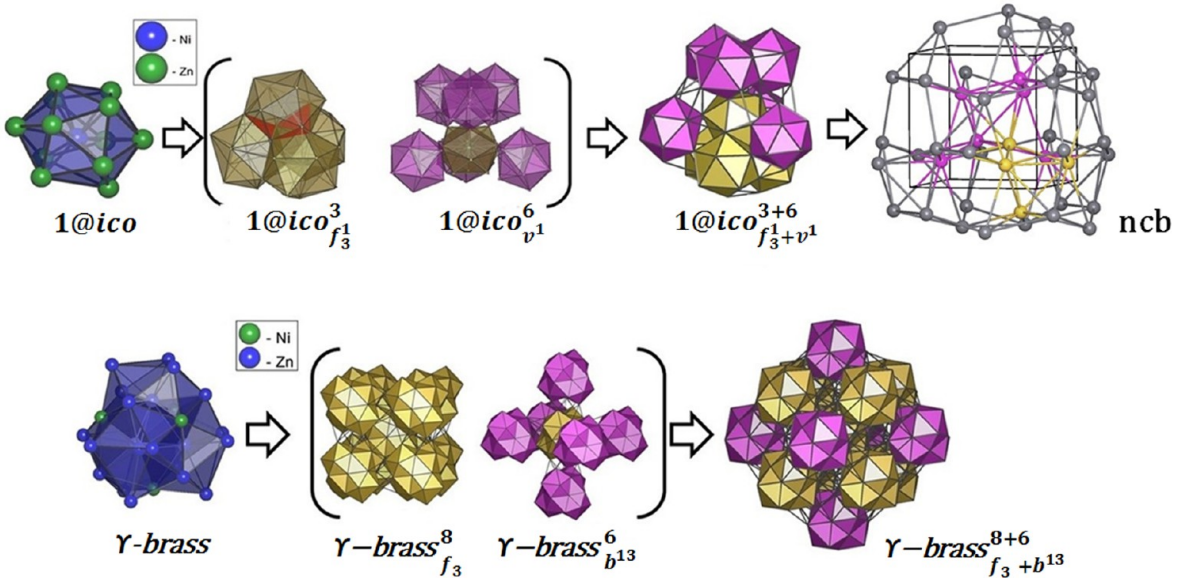

Figure 9. (top) The Ni_4Zn_{22} crystal structure: atom-centered 1@12 icosahedron (left) and the constituents (middle) of the $1@ico^{3+6}_{f_3^1+v^1}$ supracluster (right), where the central icosahedron (highlighted in red) is connected to the surrounding ones by common vertices and faces, resulting in an **ncb** underlying net. (bottom) The 0@4@22 γ-brass cluster (left) and the constituents (middle) of the γ-brass$^{8+6}_{f_3+b^{13}}$ supracluster (right), where the central icosahedron is connected to the surrounding ones by common faces and intercluster bonds.

DOI: 10.1021/acs.inorgchem.5b00960
Inorg. Chem. 2015, 54, 6616−6630

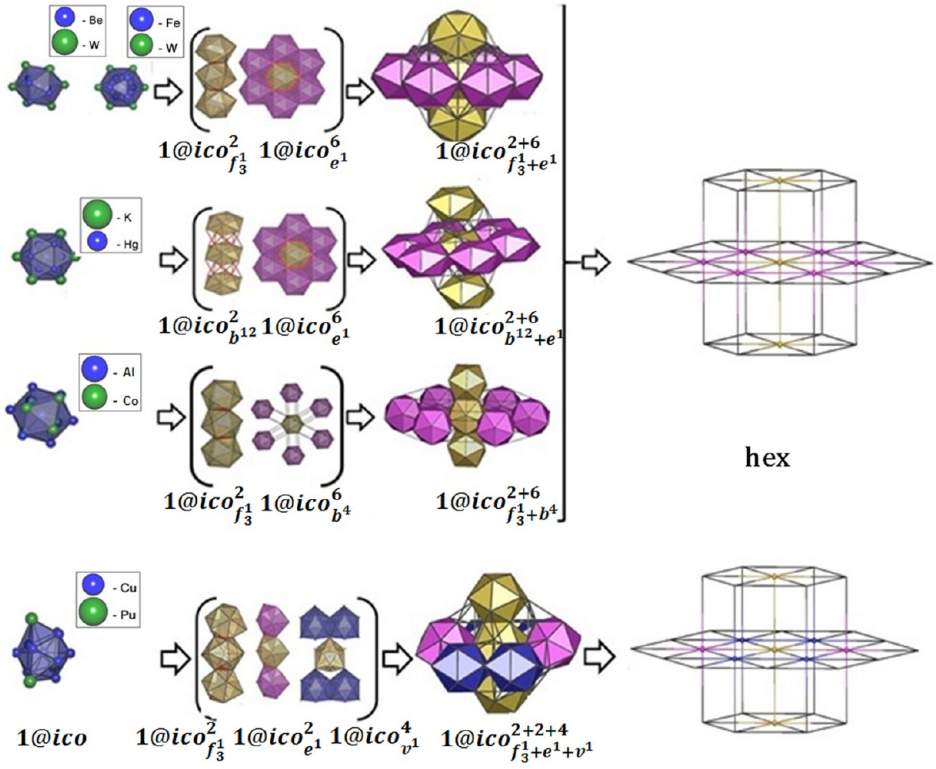

Figure 10. Atom-centered 1@12 icosahedra (left), the corresponding supraclusters (middle), and their assemblies into **hex** underlying nets (right) in the WBe_2, Fe_2Ta, K_2Hg_7, Co_2Al_5, and $PuCu_6$ crystal structures.

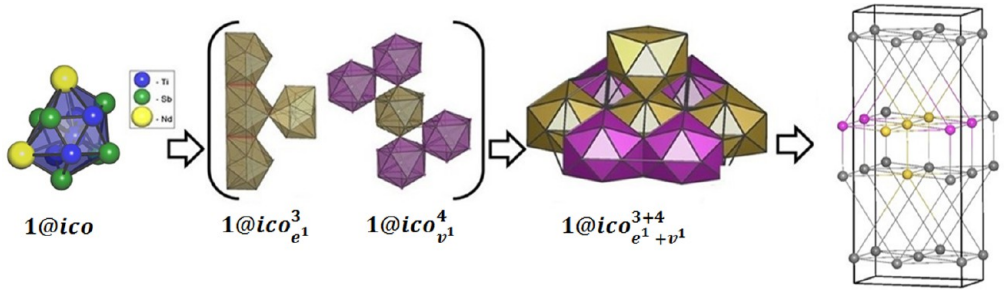

Figure 11. An atom-centered 1@12 icosahedron (left), the corresponding supracluster (middle), and the assembly of the supraclusters into a 7-coordinated $3^6.4^{12}.5^3$ underlying net (right) in the $NdTi_3(Sn_{0.1}Sb_{0.9})_4$ crystal structure.

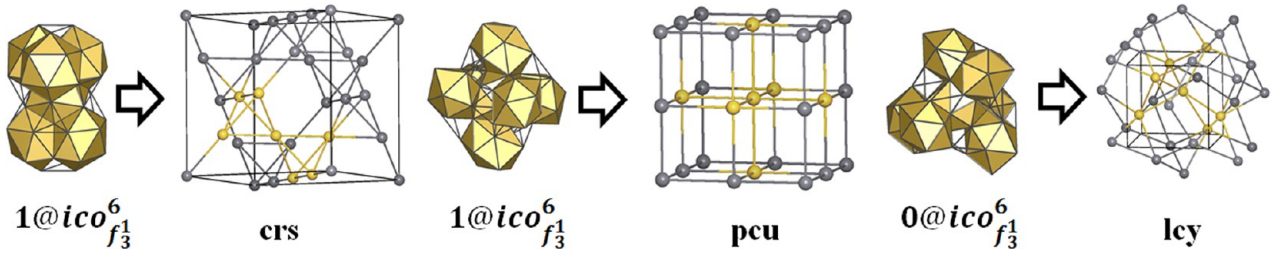

Figure 12. (left) $1@ico^6_{f_3^1}$ supracluster in the Ti_2Ni and Gd_4RhIn topological types. (middle) $1@ico^6_{f_3^1}$ supracluster in the Ca_3Ag_8 topological type. (bottom): $0@ico^6_{f_3^1}$ supracluster in the $Y_5Ag_3Cu_{12}$ topological type.

nonequivalent icosahedra (Table S3 in the Supporting Information). Eight structures of the Mn_3In, $Ag_9Ca_8Hg_9$, and $Cd_{43}Pd_8$ topological types can be constructed from two nonequivalent icosahedra of equal or similar composition: Mn@Mn9In3 (×2), Ag@Ag6Ca6 and Ag@Ag9Ca3, or Pd@Cd12 (×2), respectively, according to the same 9-c **ncb** topological scheme; the LB*ico* in all cases is $1@ico^{3+6}_{f_3^1+v^1}$. As in the case of the one-icosahedron-based intermetallics with this type of assembly (see the previous section), all eight of these structures can also be considered as an assembly of γ-brass clusters.[31] The remaining 10 and four structures are built up from two or three kinds of nonequivalent icosahedra, respectively, but their underlying nets differ from those of the one-icosahedron-based intermetallics. However, two nonequivalent icosahedra

DOI: 10.1021/acs.inorgchem.5b00960
Inorg. Chem. 2015, 54, 6616−6630

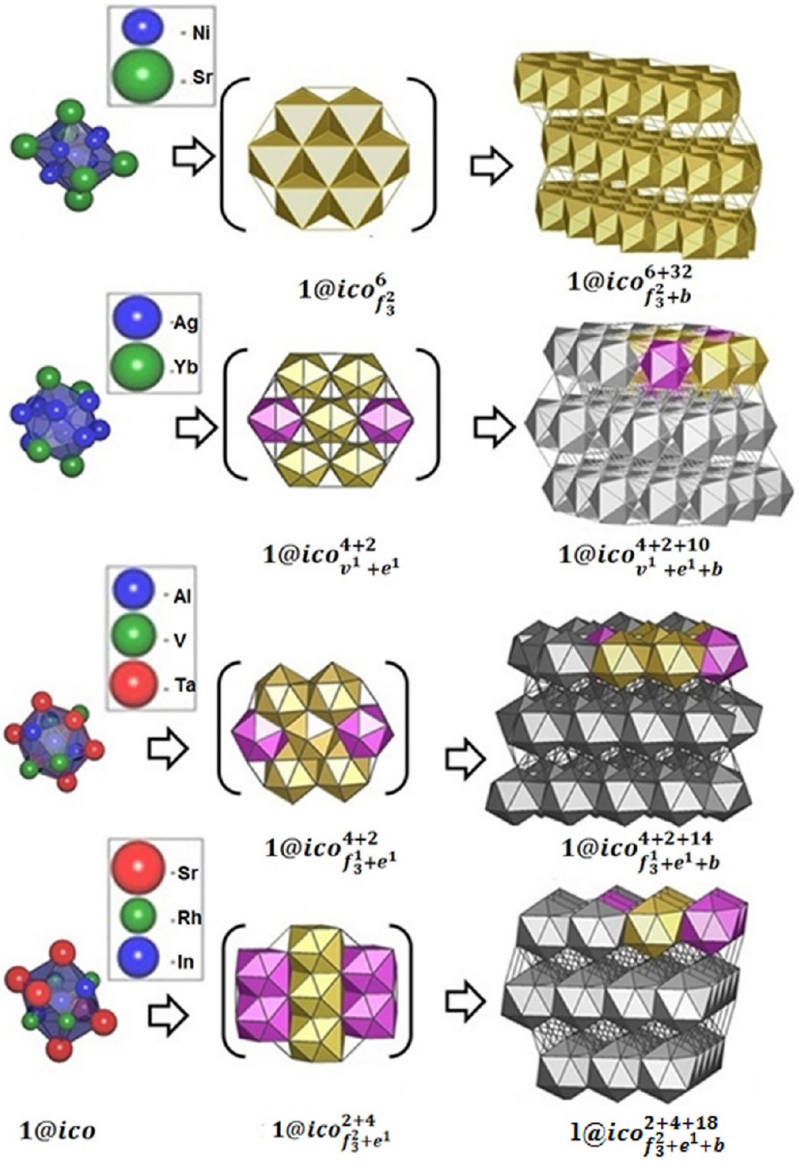

Figure 13. Atom-centered 1@12 icosahedra (left), the corresponding supraclusters (middle), and their assemblies into **hxl** underlying nets (right) in the Sr_2Ni_3, Yb_2Ag_7, $Al_{2.88}Ta_{2.66}V_{1.46}$, and $Sr_2Rh_2In_3$ crystal structures.

can construct supraclusters with known LB*ico* 1@*ico*$^{1+6+3}_{f_3^1+e^1+v^1}$ and 1@*ico*$^{2+6}_{f_3^1+e^1}$ in five structures of the (AlCu)Mg, MoNi, and $Mg_{16}Zn_{31}Cu$ topological types.

Chemical Composition of Icosahedral Building Units. In this part, we present the results of the analysis of the chemical composition of the icosahedra that constitute the entire crystal structure for 414 ordered binary or ternary intermetallics (Tables S4 and S5 in the Supporting Information). The distribution of the elements forming the icosahedra is given in Figure 14. One can see that almost any element can participate in the icosahedral nanoclusters as the central atom or in its environment. The nanoclusters with the chemical composition $A@A_6+M_6$ or $A@M_{12}$ are the most numerous for the binary intermetallics (Table S4), while $A@A_7+M_5$, $A@A_8+M_4$, and $A@A_9+M_3$ occur very rarely. For the ternary compounds, the composition $A@M^1{}_6+M^2{}_6$ is the most typical. Importantly, not all elements can form any stoichiometry of the nanocluster; in particular, such elements as Ag, Cr, Cu, Hf, K, Li, Mg, Mn, Na, Sc, Ti, and Zn play the role of the central atom only for the $A@A_6+M_6$ nanoclusters, while Bi, Ga, Ge, In, Pd, Rh, Sb, Sn, Tl, and W can be central atoms only in the $A@M_{12}$ nanoclusters in the binary intermetallics.

Expectedly, the distribution of atoms over the A and M positions (Tables S6 and S7 in the Supporting Information) depends on the atom size. In particular, in the most abundant nanoclusters, $A@M_{12}$ and $A@A_6+M_6$, the A atom is usually smaller than M; a typical ratio of radii r_A/r_M for the $A@M_{12}$ icosahedra is about 0.9, which corresponds to close packing of the spherical atoms. Exceptions are rather regular; thus, in 93% of the $A@M_{12}$ icosahedra with $r_A/r_M > 1$, the M atoms belong to groups 4−6 of the periodic table, while 89% of the structures that contain the $A@A_6+M_6$ icosahedra with $r_A/r_M > 1$ are assembled according to the **crs** underlying net. A physical model that explains such regularities remains to be developed.

Correlations between Topological Parameters and Chemical Composition. Above we have provided statistical data on chemical composition, local binding of icosahedra, and overall topological parameters; now we consider correlations between them. First of all, there is a strong conformity between the local and overall topologies. Thus, knowing LB*ico*, one can

DOI: 10.1021/acs.inorgchem.5b00960
Inorg. Chem. 2015, 54, 6616−6630

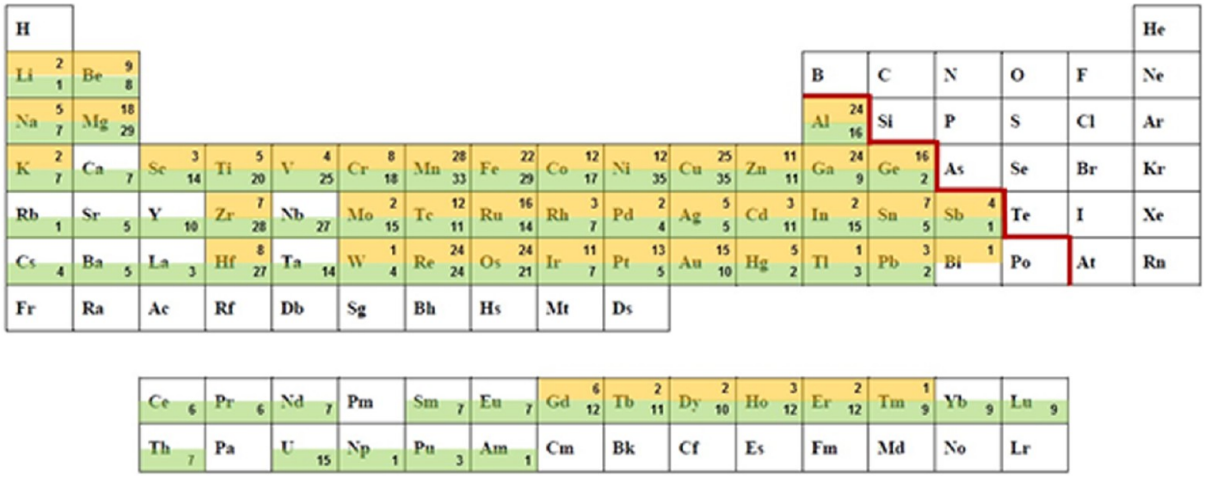

Figure 14. Atoms composing the icosahedral clusters. Central (A) and shell (M) atoms of the icosahedra are given at the top and bottom of each box and highlighted in yellow and green, respectively; the numbers in each cell show the number of structures in which the atom plays the corresponding role. The Zintl line is shown in red.

predict the overall topology of an underlying net with a high probability. For instance, if a central icosahedron is connected to two icosahedra through one triangular face and to six icosahedra through one common edge, i.e., the supracluster type is $1@ico^{2+6}_{f^1_3+e^1}$, the resulting underlying net has strictly the **hex** topology (Table S2 in the Supporting Information). In turn, the inverse task gives a less rigorous result with several choices, but still one of them has a high probability; the **hex** motif can be realized in the structures with four different LB*ico*, but with a 94.7% probability for $1@ico^{2+6}_{f^1_3+e^1}$.

At the same time, there is no strict correspondence between the topology of an underlying net and the topology of the whole structure. Obviously, intermetallics belonging to the same topological type have the same LB*ico* and underlying nets, but a given underlying net or local arrangement of icosahedra can be realized in different topological types.

The chemical composition of the icosahedra influences the underlying nets as well. For instance, icosahedra with homoatomic shells assemble the crystal structure according to the **bcu-x** motif in 94% of cases, while the **hex** underlying net is realized in $A@A_6+M_6$ icosahedra in almost 76% of cases (Table 3).

Beyond the Icosahedral Core: Bergman Clusters as Building Units in Intermetallics. In this paper, we have devoted our main attention to the simplest icosahedron-based nanocluster models, where the primary nanoclusters are icosahedra themselves; nonetheless, such models cover a good deal of intermetallic structures. These examples are useful also from the methodological point of view because the simple models can be clearly illustrated and conceived. However, the concepts and methods of the nanocluster analysis are quite universal and can be applied to much more complicated architectures. In this section, we outline how the nanocluster approach allows one to deal with intermetallic structures based on more complex primary nanoclusters with icosahedral symmetry. In particular, an empty or centered icosahedron can serve as a template for the *D*32, *D*42, or *D*50 deltahedral nanoclusters.[66−68] As an example, we analyze here the intermetallics that contain Bergman-type *D*32 structural units. The role of the Bergman nanoclusters in the assembly of the icosahedron- and deltahedron-based intermetallics was already discussed in detail in our previous works.[32,69] Here we study the local binding topologies of the Bergman-type nanoclusters as well as their ability to serve as templates for even more complicated nanoclusters.

Table 3. Relations between Chemical Composition of the Icosahedral Building Units and Motifs of Their Assembly

icosahedron composition	underlying net[a]
$A@A_6+M_6$	**hex** (158), **crs** (27); **tca** (21); **pcu** (1)
$A@M_{12}$	**bcu-x** (84), **ncb** (3); **fcu** (2)
$A@A_9+M_3$	**hex** (12); **fcu** (2), **dia** (1)
$A@A_8+M_4$	**hxl** (4)
$A@A_7+M_5$	**dia** (1)
$A@A_3+M_9$	**ncb** (2)
$0@M^1_6+M^2_6$	**hex** (7)
$0@M^1_8+M^2_4$	**bcu-x** (1)
$A@M^1_6+M^2_6$	**pcu** (17), **crs** (12), **hex** (21), **fcu** (2), **sql** (1), **hxl** (1)
$A@M^1_9+M^2_3$	**fcu** (5)
$A@A_8+M^1_2+M^2_2$	**fcu** (1)
$A@A_7+M^1_2+M^2_3$	**hex** (8)
$A@A_6+M^1_3+M^2_3$	**crs** (17)
$A@A_4+M^1_6+M^2_2$	**hex** (1)
$A@A_3+M^1_5+M^2_4$	**dia** (1)
$A@A_2+M^1_4+M^2_6$	**hxl** (1)
$A@A+M^1_5+M^2_6$	**dia** (2)

[a]The numbers of structures with the given underlying nets are shown in parentheses.

Bergman Clusters as Building Units. The Bergman cluster with a *D*32 deltahedral shell was discovered in the $Mg_{32}(Al,Zn)$ structure[70] and described as a centered inner icosahedron surrounded by a 20-atom pentagonal dodecahedron (*dod*) of with one atom above each triangular face of the icosahedron and by a 12-atom outer icosahedron with one atom above each pentagonal face of the dodecahedron (Figure 15).

Bergman-type clusters can be considered in the nanocluster approach as onionlike 44-atom 0@12@32 or 45-atom 1@12@32 two-shell nanoclusters. In addition, the TTN collection includes isomeric Bergman nanoclusters with the same composition but different systems of interatomic contacts. Below we will consider all kinds of isomeric 0@12@32 and 1@12@32 nanoclusters.

The list of 23 local binding topologies of the Bergman-based intermetallics (LB*ico*@*D*32) is presented in Table S8 in the Supporting Information and will be not discussed in detail for the sake of brevity.

DOI: 10.1021/acs.inorgchem.5b00960
Inorg. Chem. 2015, 54, 6616−6630

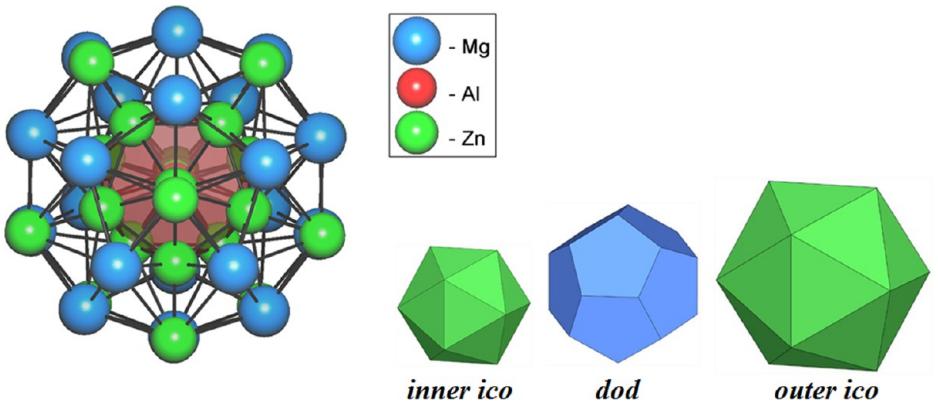

Figure 15. The 1@12@32 Bergman cluster in the $Mg_{32}(Al,Zn)$ crystal structure as a sequence of an inner icosahedron, a pentagonal dodecahedron, and an outer icosahedron.

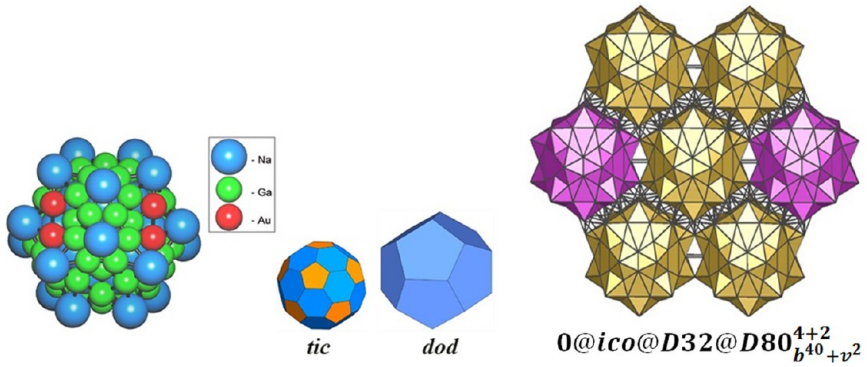

Figure 16. $Na_{128}Au_{81}Ga_{275}$ crystal structure: (left) a 0@12@32@80 nanocluster, the *D*80 shell of which can be decomposed into a truncated icosahedron and a pentagonal dodecahedron; (right) a 0@*ico*@*D*32@*D*80$^{4+2}_{b^{40}+v^2}$ supracluster.

Bergman Clusters as Templates. In the crystal structures of intermetallics, empty Bergman clusters can play the role of templates for the three-shell nanoclusters with *D*80, *D*86, *D*92, or *D*110 deltahedral third shells; atom-centered Bergman clusters can be a core for the *D*98 deltahedron.

The nanocluster with the *D*80 deltahedron in the $Na_{128}Au_{81}Ga_{275}$ structure[71] can be presented as a combination of a truncated icosahedron (*tic*, C_{60} fullerene-like) and a pentagonal dodecahedron (*dod*) (Figure 16). The hexagonal faces of the fullerene-like shell are located above the deltahedron of the 32-atomic Bergman-like shell, whereas the pentagonal faces are projected to the inner icosahedron. The 20 atoms that form the outer deltahedron are projected to the centers of the 20 hexagonal faces of the fullerene-like shell.

The $K_{49}Tl_{108}$ structure[72] has two alternative models as an assembly of 0@12@32@86 or 0@12@32@92 nanoclusters that are located in the 1*b* and 1*a* positions, respectively. The *D*86 deltahedral shell can be considered as a superposition of a 54-vertex polyhedron having 24 pentagonal and eight hexagonal faces, a pentagonal dodecahedron, and an icosahedron (Figure 17 top). The *D*92 deltahedron is formed as the following combination of nested polyhedra: a truncated icosahedron (*tic*), a pentagonal dodecahedron (*dod*), and an icosahedron (*ico*) (Figure 17 bottom). The difference between the two possible models, 0@Tl12@K20Tl12@K26Tl60 and 0@Tl12@K20Tl12@K20Tl72, is in the third shell, or rather in the first polyhedron of the third shell, of the corresponding nanoclusters. This is caused by the fact that the 60-vertex polyhedron is formed by 24 atoms of Tl1, 24 atoms of Tl2, and 12 atoms of Tl7, while the 54-vertex polyhedron is formed by 24 atoms of Tl1, 24 atoms of Tl2, and six atoms of K6. Thereby, the different arrangements of Tl7 (icosahedron) and K6 (octahedron) produce different models. In both cases, the three-shell nanoclusters are packed according to 6-coordinated **pcu** motifs with the 0@*ico*@*D*32@*D*86$^{6}_{v^1+e^4}$ or 0@*ico*@*D*32@*D*92$^{6}_{v^1+e^4}$ local binding topologies (Table S8 in the Supporting Information). Since the two models are quite similar, it is hardly possible to prefer one of them; in practice, this could mean that different structure domains are assembled with different kinds of nanoclusters, which probably coexist in the reaction medium.

In addition to the ordered fullerene-based *D*80 and *D*92 deltahedra, there is a *D*110 deltahedron, which includes a 60-atom shell corresponding to a rhombiicosidodecahedron with 12 pentagonal faces, 30 quadrangular faces and 20 triangular faces. The construction of the *D*110 deltahedron is shown for the $Au_{115.29}Ca_{24}Sn_{34.81}$ structure type[73] as a sequence of an icosidodecahedron (*ido*, 30 atoms), a cube (*cub*), a rhombiicosidodecahedron (*ric*, 60 atoms), and an icosahedron (Figure 18). The assembly of the three-shell nanoclusters is characterized by a 14-coordinated **bcu-x** underlying net, where the central 0@12@32@110 nanocluster is connected to eight other equivalent nanoclusters through 14 common triangular faces and to six nanoclusters through two common faces.

In the $Li_{33.3}Ba_{13.08}Ca_{2.96}$ crystal structure,[74] the three-shell 1@12@32@98 nanoclusters are packed according to the face-centered cubic (**fcu**) motif with the 0@*ico*@*D*32@*D*98$^{12}_{e^1}$ local binding topology (Figure 19).

DOI: 10.1021/acs.inorgchem.5b00960
Inorg. Chem. 2015, 54, 6616−6630

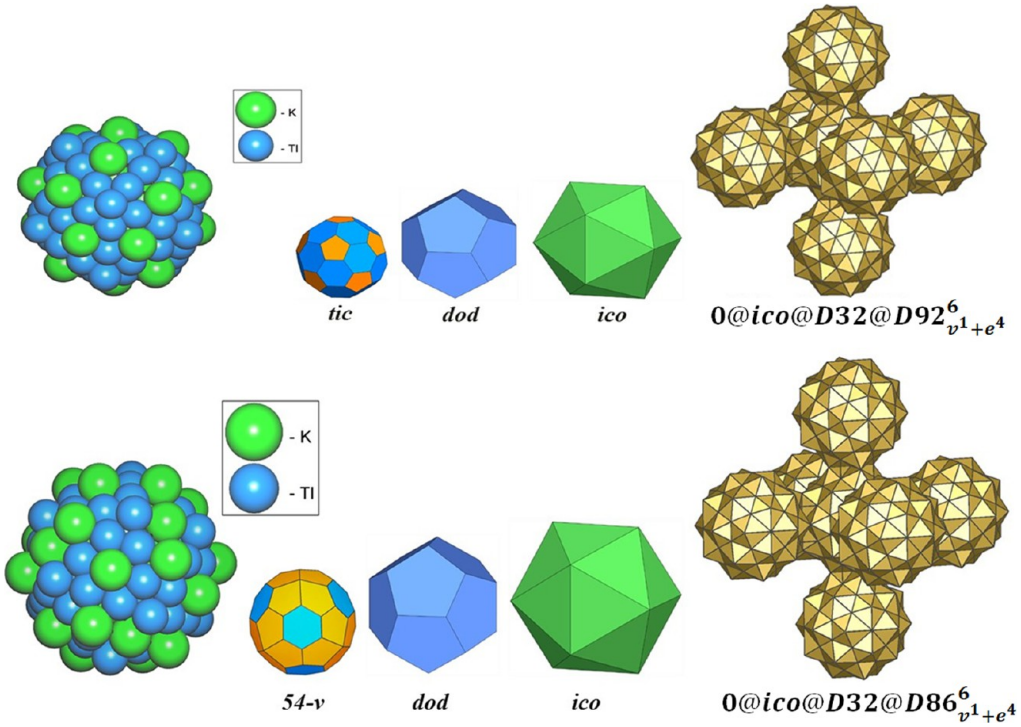

Figure 17. Two nanocluster models of the $K_{49}Tl_{108}$ crystal structure: (top left) a 0@12@32@92 nanocluster, the *D*92 shell of which can be decomposed into a truncated icosahedron, a pentagonal dodecahedron, and an icosahedron; (top right) a 0@*ico*@*D*32@*D*92$^{6}_{v^1,e^4}$ supracluster; (bottom left) a 0@12@32@86 nanocluster, the *D*86 deltahedral shell of which can be represented as a sequence of a 54-vertex polyhedron, a pentagonal dodecahedron, and an icosahedron; (right) a 0@*ico*@*D*32@*D*86$^{6}_{v^1,e^4}$ supracluster.

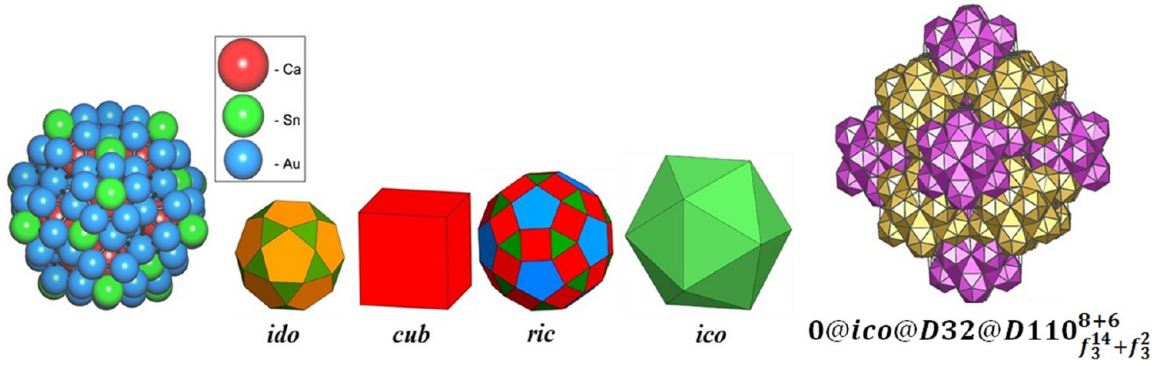

Figure 18. Structural units in the $Au_{115.29}Ca_{24}Sn_{34.81}$ crystal structure: (left) a 0@12@32@110 nanocluster, the *D*110 deltahedral shell of which is represented as a sequence of an icosidodecahedron, a cube, a rhombiicosidodecahedron, and an icosahedron; (right) a 0@*ico*@*D*32@*D*110$^{8+6}_{f_3^{14}+f_3^2}$ supracluster.

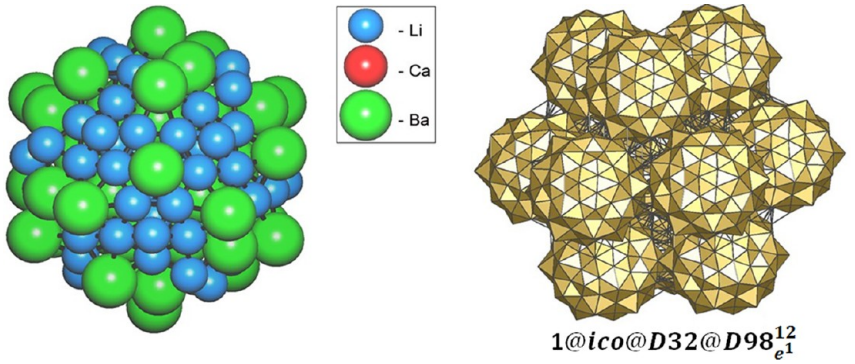

Figure 19. $Li_{33.3}Ba_{13.08}Ca_{2.96}$ crystal structure: (left) a 1@12@32@98 nanocluster; (right) a 1@*ico*@*D*32@*D*98$^{12}_{e^1}$ supracluster.

The analysis of the icosahedron-based nanoclusters shows that they can be associated with multishell nanoclusters consisting of high-symmetry shells in the form of *D*32, *D*80, *D*86, *D*92, *D*98, or *D*110 deltahedra, where 32, 80, 86, 92, 98,

DOI: 10.1021/acs.inorgchem.5b00960
Inorg. Chem. 2015, 54, 6616−6630

and 110 are the numbers of atoms in the shell. Icosahedra can play the role of a template on which the *D*32 deltahedron is formed, and in turn, on its surface five types of shells are built in the form of *D*80, *D*86, *D*92, *D*98, and *D*110 deltahedra. The shell-by-shell growth of icosahedron-based nanoclusters with the Bergman-type *D*32 core is presented in Scheme 2.

Scheme 2. Genetic Tree of the N_1@12@32@N_2 Metallic Icosahedron-Based Nanoclusters from 12 to 154 Atoms with the Bergman-Type *D*32 Core; The Growth of the Nanocluster Shells Is Shown in Two Kinds of Operation: "+CC" for Adding a Central Atom and "+@" for Adding a Shell

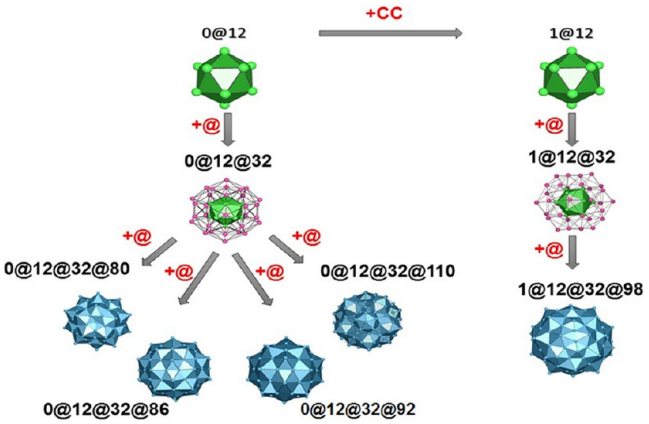

From the TTN Collection to a Knowledge Database and an Expert System. In the next step of our future work we are going to include the information about the distributions of the topological parameters and their correlations to the TTN collection and transform it to a knowledge database of an expert system. The expert system can be used to predict possible motifs of building units in intermetallics and further to provide expert conclusions about possible new intermetallic compounds and their structural features.

As was mentioned above, such a knowledge database will consist of three levels of data. The first level contains experimental crystal data for intermetallics from the ICSD and Pearson Crystal Data. The second one is the TTN collection, which comprises chemical, topological, and geometrical parameters of building units and the methods of their assembly (underlying nets). The third level includes the information about relations between the parameters accumulated in the TTN collection. The descriptors involved in the relations could be as follows:

(i) nanocluster type, i.e., the geometry of a nanocluster with the particular number of vertices, edges, and faces;
(ii) type of the central atom for a given nanocluster type;
(iii) chemical composition of the environment of the central atom;
(iv) local symmetry of the nanocluster in the crystal structure;
(v) maximum point symmetry of the nanocluster itself;
(vi) local topology of the nanocluster binding;
(vii) overall topology of the nanocluster assembly (underlying net);
(viii) space group, crystal system, crystal class, and other crystallographic descriptors.

The expert system will use the relations between these descriptors to provide an expert conclusion resting upon the required parameters specified by the user.

Let us illustrate how the expert system can be applied to predict the structural features of icosahedron-based intermetallics. First, the user should specify the primary nanoclusters (icosahedra); they can be chosen from the list provided by the TTN collection. Then the user can restrict the crystal symmetry, which can sharply increase the robustness of the prediction. Thus, the **hex** topology of the underlying net is preferable for hexagonal crystal systems and occurs in 771 such structures (90.4%); among the remaining structures, the **tca** and **fcu** motifs are realized in 81 (9.5%) and 1 (0.1%) (Tables S9 and S10 in the Supporting Information). By further specifying the information on the supracluster type, the user allows the expert system to unambiguously answer the question "what topology of the underlying net does this system have?"; assembly of icosahedra into the supracluster by sharing of faces and edges or sharing of faces and bonds give rise to the **hex** underlying topology, while **tca** is obtained from the assembly of icosahedra by sharing of faces and edges.

In some cases, the information about chemical composition can be crucial in predicting the underlying net. In particular, the A@M_{12} composition is realized in 96.6% of cases as a **bcu-x** motif. If we consider the Co@Co_6+M_6 composition, the **tca** (42.9%) and **hex** (42.9%) motifs compete with each other, and the **crs** underlying net is realized in 14.2% cases; in all of them, the M atom is larger than the central one (Tables S4 and S5 in the Supporting Information).

These examples illustrate the main idea of the knowledge database and the expert system. The knowledge database accumulates a lot of more-or-less general correlations among many chemical, structural, and other descriptors (e.g., physical properties of crystals can be added to the list). Some of these correlations can be well-known to the human expert, but nobody can keep all of them in mind as the knowledge database does, and nobody can apply all of them to a particular task as the expert system can do. Altogether, these computer tools can essentially help the researcher in the design of new intermetallic structures.

CONCLUSION

Usually the structure of intermetallic compounds is described in terms of coordination polyhedra of atoms; hence, the description does not go beyond the first coordination shell. Other structural units have been considered occasionally, but there have been no systematic studies of the nanoscale local domains or the methods of assembling these domains into periodic structures. The TTN collection announced in this paper and the method of nanoclustering analysis are intended to be tools for such studies; they make possible the systematic exploration of both local and overall motifs of any complexity in an automated mode. This is a way to reveal structural regularities on a new level and to predict some structure features resting upon data-mining approaches. As a result, the TTN collection should be transformed into a knowledge database that can then be used in an expert system to assist the experimentalist in the design of new intermetallic compounds.

ASSOCIATED CONTENT

Supporting Information

Table S1 contains graphs of 0@12 and 1@12 nanoclusters and their occurrence in intermetallics. Tables S2 and S3 present the distributions of local binding of icosahedra in intermetallics assembled with one nonequivalent icosahedron and two or three nonequivalent icosahedra, respectively. Tables S4 and S5

DOI: 10.1021/acs.inorgchem.5b00960
Inorg. Chem. 2015, 54, 6616−6630

list the distributions of chemical elements in binary and ternary intermetallics, respectively, assembled with one nonequivalent icosahedron. Tables S6 and S7 contain the distributions of chemical elements among central atoms and environment atoms in the centered icosahedra. Table S8 presents a distribution of local binding of Bergman and Bergman-based clusters in intermetallics. Tables S9 and S10 present correlations between the underlying net topology and the crystal system. The Supporting Information is available free of charge on the ACS Publications website at DOI: 10.1021/acs.inorgchem.5b00960.

AUTHOR INFORMATION

Corresponding Author

*Phone: +7-8463356798. Fax: +7-8463345417. E-mail: blatov@samsu.ru.

Notes

The authors declare no competing financial interest.

ACKNOWLEDGMENTS

The authors are grateful to the Russian Government (Grant 14.B25.31.0005) and the Russian Foundation for Basic Research (Grant 13-07-00001) for support.

REFERENCES

(1) Pearson, W. B. *The Crystal Chemistry and Physics of Metals and Alloys*; Wiley-Interscience: New York, 1972.
(2) Hellner, E.; Koch, E. *Acta Crystallogr.* **1981**, *A37*, 1−6.
(3) Chabot, B.; Cenzual, K.; Parthé, E. *Acta Crystallogr.* **1981**, *A37*, 6−11.
(4) Nyman, H.; Andersson, S. *Acta Crystallogr.* **1979**, *A35*, 580−583.
(5) Lord, E. A.; Ranganathan, S. *J. Non-Cryst. Solids.* **2004**, *334*−*335*, 121−125.
(6) Lord, E. A.; Mackay, A. L.; Ranganathan, S. *New Geometries for New Materials*; Cambridge University Press: Cambridge, U.K., 2006.
(7) Damasceno, P. F.; Engel, M.; Glotzer, S. C. *Science* **2012**, *337*, 453−457.
(8) Damasceno, P. F.; Engel, M.; Glotzer, S. C. *ACS Nano* **2012**, *6*, 609−614.
(9) Samson, S. *Nature* **1962**, *195*, 259−262.
(10) Samson, S. *Acta Crystallogr.* **1964**, *17*, 491−495.
(11) Samson, S. *Acta Crystallogr.* **1965**, *19*, 401−413.
(12) Kreiner, G.; Franzen, H. F. *J. Alloys Compd.* **1997**, *259*, 83−114.
(13) Yang, Q.-B.; Andersson, S.; Stenberg, L. *Acta Crystallogr.* **1987**, *B43*, 14−16.
(14) Bergman, G. *Acta Crystallogr.* **1996**, *B52*, 54−58.
(15) Fredrickson, D. C.; Lee, S.; Hoffmann, R. *Angew. Chem., Int. Ed.* **2007**, *46*, 1958−1976.
(16) Feuerbacher, M.; Thomas, C.; Makongo, J. P. A.; Hoffmann, S.; Carrillo-Cabrera, W.; Cardoso, R.; Grin, Y.; Kreiner, G.; Joubert, J.-M.; Schenk, T.; Gastaldi, J.; Nguyen-Thi, H.; Mangelinck-Noël, N.; Billia, B.; Donnadieu, P.; Czyrska-Filemonowicz, A.; Zielinska-Lipiec, A.; Dubiel, B.; Weber, T.; Schaub, P.; Krauss, G.; Gramlich, V.; Christensen, J.; Lidin, S.; Fredrickson, D.; Mihalkovic, M.; Sikora, W.; Malinowski, J.; Brühne, S.; Proffen, T.; Assmus, W.; de Boissieu, M.; Bley, F.; Chemin, J.-L.; Schreuer, J.; Steurer, W. *Z. Kristallogr.* **2007**, *222*, 259−288.
(17) Shevchenko, V. Ya.; Blatov, V. A.; Ilyushin, G. D. *Struct. Chem.* **2009**, *20*, 975−982.
(18) Suck, J.-B.; Schreiber, M.; Haussler, P. *Quasicrystals: An Introduction to Structure, Physical Properties and Applications*; Springer: Berlin, 2002.
(19) Trebin, H.-R. *Quasicrystals: Structure and Physical Properties*; Wiley-VCH: Weinheim, Germany, 2003.
(20) Senechal, M.; Taylor, J. E. *Math. Intelligencer* **2013**, *35*, 1−9.
(21) Doye, J. P. K.; Wales, D. J. *New J. Chem.* **1998**, *22*, 733−744.
(22) Doye, J. P. K. *Comput. Mater. Sci.* **2006**, *35*, 227−231.
(23) Zhan, L.; Chen, J. Z. Y.; Liu, W.-K.; Lai, S. K. *J. Chem. Phys.* **2005**, *122*, No. 244707.
(24) Elliott, J. A.; Shibuta, Y.; Wales, D. J. *Philos. Mag.* **2009**, *89*, 3311−3332.
(25) Fernández, E. M.; Soler, J. M.; Garzón, I. L.; Balbás, L. C. *Phys. Rev. B* **2004**, *70*, No. 165403.
(26) Wales, D. J.; Doye, J. P. K.; Dullweber, A.; Hodges, M. P.; Naumkin, F. Y.; Calvo, F.; Hernández-Rojas, J.; Middleton, T. F. The Cambridge Cluster Database. http://www-wales.ch.cam.ac.uk/CCD.html (accessed April 29, 2015).
(27) Delgado-Friedrichs, O.; O'Keeffe, M. *J. Solid State Chem.* **2005**, *178*, 2480−2485.
(28) Blatov, V. A. *Struct. Chem.* **2012**, *23*, 955−963.
(29) Blatov, V. A.; Shevchenko, A. P.; Proserpio, D. M. *Cryst. Growth Des.* **2014**, *14*, 3576−3586. Also see: http://topospro.com/.
(30) O'Keeffe, M.; Peskov, M. A.; Ramsden, S. J.; Yaghi, O. M. *Acc. Chem. Res.* **2008**, *41*, 1782−1789. Also see: http://rcsr.anu.edu.au/.
(31) Pankova, A. A.; Blatov, V. A.; Ilyushin, G. D.; Proserpio, D. M. *Inorg. Chem.* **2013**, *52*, 13094−13107.
(32) Pankova, A. A.; Ilyushin, G. D.; Blatov, V. A. *Crystallogr. Rep.* **2012**, *57*, 1−9.
(33) Jana, P. P.; Pankova, A. A.; Lidin, S. *Inorg. Chem.* **2013**, *52*, 11110−11117.
(34) Mahne, S.; Harbrecht, B. *J. Alloys Compd.* **1994**, *203*, 271−279.
(35) Mitina, T. G.; Blatov, V. A. *Cryst. Growth Des.* **2013**, *13*, 1655−1664.
(36) Shoemaker, D. P.; Shoemaker, C. B. In *Introduction to Quasicrystals*; Jarić, M. V., Ed.; Academic Press: San Diego, CA, 1988; Chapter 1.
(37) Wallbaum, H. J. *Z. Kristallogr.* **1941**, *103*, 391−402.
(38) Wallbaum, H. J. *Naturwissenschaften* **1942**, *30*, 149.
(39) Adam, J.; Rich, J. B. *Acta Crystallogr.* **1954**, *7*, 813−816.
(40) Pan, V. M.; Latysheva, V. I.; Kulik, O. G.; Gorskii, V. V. *Russ. Metall.* **1982**, 195−198.
(41) Linsinger, S.; Eul, M.; Rodewald, U. C.; Pöttgen, R. *Z. Naturforsch., B* **2010**, *65*, 1185−1190.
(42) Fornasini, L.; Merlo, F. J. *J. Less-Common Met.* **1988**, *142*, 289−294.
(43) Hlukhyy, V.; Fässler, T. F. *Z. Anorg. Allg. Chem.* **2008**, *634*, 2316−2322.
(44) Siggelkow, L.; Hlukhyy, V.; Fässler, T. F. *Z. Anorg. Allg. Chem.* **2010**, *636*, 1870−1879.
(45) Buchler, H.; Range, K. J. *J. Less-Common Met.* **1990**, *161*, 347−354.
(46) Johansson, A.; Ljung, H.; Westman, S. *Acta Chem. Scand.* **1968**, *22*, 2743−2753.
(47) Brandon, J. K.; Brizard, R. Y.; Chieh, P. C.; McMillan, R. K.; Pearson, W. B. *Acta Crystallogr.* **1974**, *B30*, 1412−1417.
(48) Thimmaiah, S.; Miller, G. J. *Chem.—Eur. J.* **2010**, *16*, 5461−5471.
(49) Misch, L. *Metallwirtsch., Metallwiss., Metalltech.* **1936**, *15*, 163−166.
(50) Vrtis, M. L.; Jorgensen, J. D.; Hinks, D. G. *Physica B+C* **1986**, *136*, 489−492.
(51) Biehl, K.; Dieseroth, H. J. *Z. Anorg. Allg. Chem.* **1999**, *625*, 1337−1342.
(52) Newkirk, J. B.; Black, P. J.; Damjanovic, A. *Acta Crystallogr.* **1961**, *14*, 532−533.
(53) Haiying, B.; Devon Moore, S. H.; Pierceya, D. G.; Tkachuk, A. V.; Zelinska, O. Ya.; Mar, A. *J. Solid State Chem.* **2007**, *180*, 2216−2224.
(54) Rostoker, W. *Trans. Am. Inst. Min., Metall. Pet. Eng.* **1952**, *194*, 209−210.
(55) Zaremba, R.; Rodewald, U. C.; Hoffmann, R. D.; Pöttgen, R. *Monatsh. Chem.* **2007**, *138*, 523−528.
(56) Calvert, L. D.; Rand, C. *Acta Crystallogr.* **1964**, *17*, 1175−1176.
(57) Zeng, L.; Li, D.; Zhuang, Y. *Acta Crystallogr.* **1993**, *C49*, 1559−1561.

DOI: 10.1021/acs.inorgchem.5b00960
Inorg. Chem. 2015, 54, 6616−6630

(58) Höhn, P.; Agrestini, S.; Baranov, A.; Hoffmann, S.; Kohout, M.; Nitsche, F.; Wagner, F. R.; Kniep, R. *Chem.—Eur. J.* **2011**, *17*, 3347−3351.
(59) Cordier, G.; Henseleit, R. *Z. Kristallogr.* **1991**, *194*, 146−147.
(60) Snyder, G. J.; Simon, A. *J. Alloys Compd.* **1995**, *223*, 65−69.
(61) Buschow, K. H. J.; Wernick, J. H.; Chin, G. Y. *J. Less-Common Met.* **1978**, *59*, 61−67.
(62) Dattagupta, J. K.; Schubert, K. *Z. Metallkd.* **1973**, *64*, 789−792.
(63) Harbrecht, B.; Rheindorf, N.; Wagner, V. *J. Alloys Compd.* **1996**, *234*, 6−11.
(64) Hoffmann, R. D.; Kussmann, D.; Pöttgen, R. *Int. J. Inorg. Mater.* **2000**, *2*, 135−141.
(65) Kirihara, K.; Nagata, T.; Kiura, K.; Kato, K.; Takata, M.; Nishibori, E.; Sakata, M. *Phys. Rev. B* **2003**, *68*, No. 014205.
(66) Bergman, G.; Waugh, J. L. T.; Pauling, L. *Acta Crystallogr.* **1957**, *10*, 254−259.
(67) Mackay, A. L. *Acta Crystallogr.* **1962**, *15*, 916−918.
(68) Blatov, V. A.; Ilyushin, G. D.; Proserpio, D. M. *Inorg. Chem.* **2010**, *49*, 1811−1818.
(69) Blatov, V. A.; Ilyushin, G. D.; Proserpio, D. M. *Inorg. Chem.* **2011**, *50*, 5714−5724.
(70) Bergman, G.; Waugh, J. L. T.; Pauling, L. *Acta Crystallogr.* **1957**, *10*, 254−259.
(71) Tillard-Charbonnel, M.; Belin, C.; Chouaibi, N. *Z. Kristallogr.* **1993**, *206*, 310−312.
(72) Cordier, G.; Müller, V.; Fröhlich, R. *Z. Kristallogr.* **1993**, *203*, 148−149.
(73) Lin, Q.; Corbett, J. D. *Inorg. Chem.* **2010**, *49*, 10436−10444.
(74) Smetana, V.; Babizhetskyy, V.; Hoch, C.; Simon, A. *J. Solid State Chem.* **2007**, *180*, 3302−3309.

DOI: 10.1021/acs.inorgchem.5b00960
Inorg. Chem. 2015, 54, 6616−6630